**The EMBO Journal** Vol.17 No.10 pp.2947–2960, 1998

# The crystal structure of asparaginyl-tRNA synthetase from *Thermus thermophilus* and its complexes with ATP and asparaginyl-adenylate: the mechanism of discrimination between asparagine and aspartic acid

**Carmen Berthet-Colominas, Laurence Seignovert, Michael Hartlein, Morten Grotli[1,2], Stephen Cusack[3] and Reuben Leberman**

European Molecular Biology Laboratory, Grenoble Outstation, BP 156X, F-38042 Grenoble, Cedex 9, France and [1]European Molecular Biology Laboratory, Postfach 1022.40, D-69012 Heidelberg, Germany

[2]Present address: Department of Chemistry, Carlsberg Laboratory, Gamle Carlsberg Vej 10, D-2500 Valby, Denmark

[3]Corresponding author

**The crystal structure of *Thermus thermophilus* asparaginyl-tRNA synthetase has been solved by multiple isomorphous replacement and refined at 2.6 Å resolution. This is the last of the three class IIb aminoacyl-tRNA synthetase structures to be determined. As expected from primary sequence comparisons, there are remarkable similarities between the tertiary structures of asparaginyl-tRNA synthetase and aspartyl-tRNA synthetase, and most of the active site residues are identical except for three key differences. The structure at 2.65 Å of asparaginyl-tRNA synthetase complexed with a non-hydrolysable analogue of asparaginyl-adenylate permits a detailed explanation of how these three differences allow each enzyme to discriminate between their respective and very similar amino acid substrates, asparagine and aspartic acid. In addition, a structure of the complex of asparaginyl-tRNA synthetase with ATP shows exactly the same configuration of three divalent cations as previously observed in the seryl-tRNA synthetase–ATP complex, showing that this a general feature of class II synthetases. The structural similarity of asparaginyl- and aspartyl-tRNA synthetases as well as that of both enzymes to the ammonia-dependent asparagine synthetase suggests that these three enzymes have evolved relatively recently from a common ancestor.**

*Keywords*: aminoacyl-tRNA synthetase/asparagine/ATP/enzyme specificity/X-ray crystallography

## Introduction

The classification of the aminoacyl-tRNA synthetases into two classes, indicating two evolutionary families of enzymes, was first based on the comparison of their primary structures (Eriani *et al.*, 1990) and confirmed by the determination of the tertiary structure of the seryl-tRNA synthetase of *Escherichia coli* (Cusack *et al.*, 1990). This demonstrated that the designated class II enzymes contained a catalytic domain based on a six-stranded antiparallel β-sheet instead of a Rossmann nucleotide-binding fold found in class I enzymes. Since then, this classification has been refined and, based on primary, tertiary and quartenary structure considerations, each class can now be subdivided into sub-classes containing more closely related enzymes (Cusack *et al.*, 1991; Moras, 1991; Cusack, 1995). There are three class IIb aminoacyl-tRNA synthetases, for the amino acids aspartic acid, lysine and asparagine. Three-dimensional structures for representative examples of the first two have been determined by X-ray crystallography (Ruff *et al.*, 1991; Delarue *et al.*, 1994; Onesti *et al.*, 1995; Cusack *et al.*, 1996). These show that the structure of these enzymes is modular, consisting of a C-terminal catalytic domain and an N-terminal anticodon-binding domain separated by a small 'hinge' region.

The expression, purification and crystallization of the recombinant asparaginyl-tRNA synthetase from the extreme thermophile *Thermus thermophilus* (Seignovert *et al.*, 1996; Berthet-Colominas *et al.*, 1997) has enabled us to undertake a structural analysis of the third synthetase of class IIb. This structure is of special interest since the comparison with the homologous aspartyl-tRNA synthetase structure provides information on how synthetases can discriminate between structurally closely related amino acids. Besides contributing to our knowledge of the structures of representative examples of the enzymes for the 20 natural amino acids, it may also enable us to build model structures for other asparaginyl-tRNA synthetases being studied in this laboratory which have not yielded crystals for structural analysis. In this context are the asparaginyl-tRNA synthetases associated with pathological conditions such as the protective antigen of the filarial nematode *Brugia malayi* (Kron *et al.*, 1995) and the human cytosolic enzyme implicated in an autoimmune syndrome (Hirakata *et al.*, 1996; Beaulande *et al.*, 1998)

## Results

The structure of asparaginyl-tRNA synthetase presented below is based on a model obtained by refining the 2.6 Å X-ray diffraction data from crystals of an isomorphous uranium derivative since this was the best data available (see Table II). The structure is not significantly different from that obtained using data at 2.8 Å resolution from native crystals. The model has tightly restrained geometry (r.m.s. bond and angle deviations of 0.005 Å and 1.228°, respectively) and is refined to an *R*-factor of 20.8% and an *R*-free of 25.3%. The Ramachandran plot shows 91.3% of residues in the most favoured regions, 8.5% in additionally allowed regions, no residues in generously allowed regions and one well-ordered residue (Ala198) consistently in a disallowed region (program Procheck; Laskowski *et al.*, 1993). The polypeptide chain of the protein subunit has been traced completely although loops 161–168, 175–

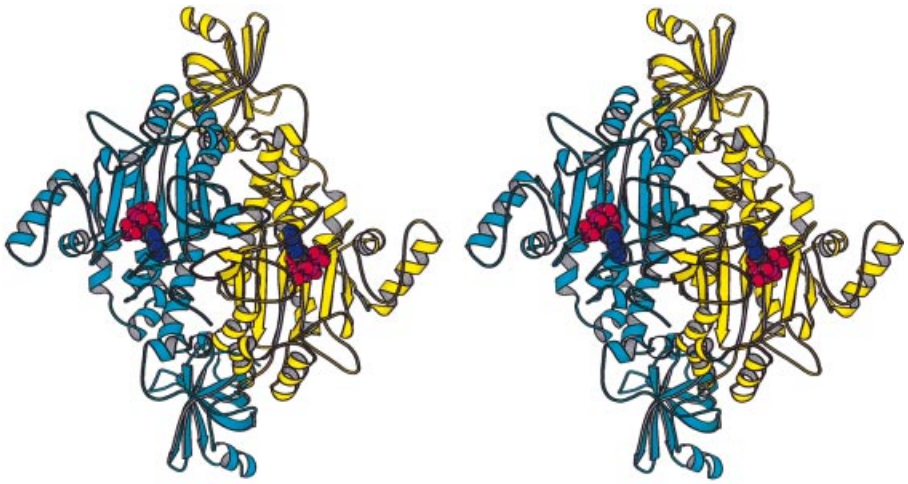

**Fig. 1.** Stereo ribbon diagram of dimer of *T.thermophilus* asparaginyl-tRNA synthetase complexed with ATP. One subunit is coloured yellow, the other cyan.

178 and 210–217 have poor or non-existent density in the native enzyme, but become more ordered in certain of the substrate complexes.

### *Structure of T.thermophilus asparaginyl-tRNA synthetase*

Asparaginyl-tRNA synthetase is a homodimeric enzyme ($\alpha 2$) with 438 amino acid residues per subunit. Figure 1 shows a ribbon representation of the three-dimensional structure of the dimer with ATP bound in the active site. Figure 2 shows an alignment of representative asparaginyl-tRNA synthetases from different organisms together with the secondary structure assignment of the *T.thermophilus* enzyme (AsnRSTT). As expected from sequence alignments, the enzyme is very similar in overall structure to the other members of the sub-class IIb enzymes of known structure, aspartyl-tRNA synthetase from yeast (AspRSSC; Ruff *et al*., 1991) and from *T.thermophilus* (AspRSTT; Delarue *et al*., 1994), and lysyl-tRNA synthetase from *E.coli* (LysRSEC; Onesti *et al*., 1995) and *T.thermophilus* (LysRSTT; Cusack *et al*., 1996). For each of the class IIb synthetases, the subunit consists of an N-terminal β-barrel anticodon-binding domain followed by a small hinge region connecting to the larger C-terminal catalytic domain, with a more variable insertion domain between the sequence motifs 2 and 3. These structural features are compared between the three class IIb synthetase subunits in Figure 3A, in which all the molecules have been placed in the same orientation by superposing their catalytic domains. The r.m.s. deviation after superposing the catalytic domains of AsnRSTT with those of AspRSSC and LysRSTT are respectively 1.37 Å (290/338 Cα $<$3 Å, 28% sequence identity) and 1.39 Å (221/324 $<$3 Å, 21% sequence identity).

### *The N-terminal domain*

The N-terminal domain which is implicated in anticodon recognition comprises residues 1–97. This domain comprises a five-stranded β-barrel (strands S1, S2, S3, S4 and S5) with an α-helix (H0) inserted between the strands S3 and S4. The same topology is observed in all class IIb synthetases, with only the N-terminal segment preceding the S1 strand being variable amongst the three enzymes. In asparaginyl-tRNA synthetase, this is a peptide of 12 amino acids including a $3_{10}$ helix (residues 5–11) which could only be built satisfactorily with reference to the electron density map of the tetragonal crystal form.

As pointed out previously, the orientation between the N- and C-terminal domains is rather variable amongst class IIb synthetases, and even between the same enzyme from different organisms (Delarue *et al*., 1994; Onesti *et al*., 1995; Cusack *et al*., 1996). If we superpose the catalytic domain of AsnRSTT on that of AspRSTT or AspRSSC, we find that the difference in orientation of the N-terminal domains is respectively 15.6° and 18.8° (Figure 3B). Comparison of the lysyl-tRNA synthetases from *E.coli* and *T.thermophilus* (Cusack *et al*., 1996) indicates that despite the variable orientation of the N-terminal domain there are conserved inter-domain interactions with the C-terminal domain of the other subunit of the dimer. In asparaginyl-tRNA synthetase, the same type of interactions are found, for instance, between Trp21 (Arg59 in LysRSTT) and the main chains of Gly399 (Gly448 in LysRSTT), and betweeen Arg37 (Leu65) and the main chain of Leu195 (Val232 in LysRSTT). That the orientation of the N-terminal domain in AsnRSTT is not dependent on crystal packing is apparent from the fact that it is not significantly different in three different crystal forms ($P4_32_12$, $P6_422$ and $P3_121$; see Materials and methods) with different packing. However, there is a small change in relative orientation upon binding of asparaginyl-adenylate which may be of functional significance (see below).

### *The interconnection region*

Residues 97–123 connect the N-terminal domain to the C-terminal domain. The connection between the two domains is made up of a turn (97–110) followed by two short α-helices H1 (111–117) and H2 (119–123) similar to that found in lysyl-tRNA synthetases (Figure 3A). In the aspartyl-tRNA synthetases, this region is longer and more globular, with three α-helices for the *T.thermophilus* enzyme and four for the yeast enzyme; in each case, the two C-terminal helices correspond to those found in the asparaginyl and lysyl enzymes.

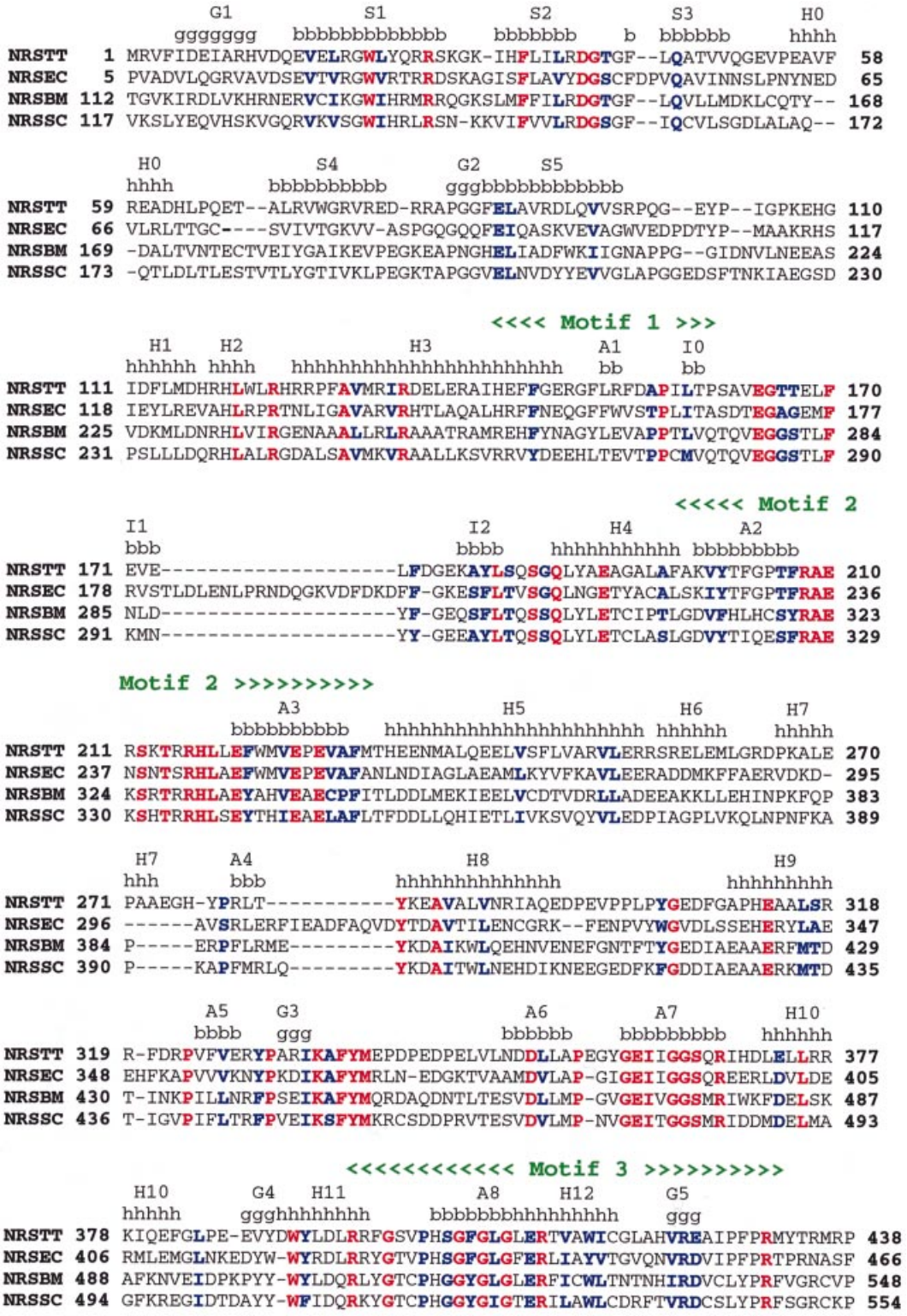


**Fig. 2.** Alignment of two prokaryote and two eukaryote asparaginyl-tRNA synthetase sequences with superposed secondary structure of the *T.thermophilus* enzyme (NRSTT). The colour code is based on an analysis of the following 10 asparaginyl-tRNA synthetase sequences (complete alignment not shown, DDBJ/EMBL/GenBank accession No. given) NRSBM, antigen of *B.malayi*, J03971; SC, *Saccharomyces cerevisiae*, X59720; TT, *T.thermophlius*, X91009; BS, *Bacillus subtilis*, L47709; LB, *Lactobacillus bulgaricus*, X89439; EC, *Escherichia coli*, X68192; SS, *Synechocystis* sp, D64006; HI, *Haemophilus influenzae*, U32810; MG, *Mycoplasma genitalium*, U39690. Red indicates residues strictly conserved for all 10 enzymes, dark blue indicates residues conserved for all 10 enzymes according to Dayhoff classes (C/HRK/FYW/DENQ/LIVM/GATSP).

### *The C-terminal domain*

The C-terminal domain, comprising residues 123–438, has an α–β fold and contains the conserved class II catalytic domain as well as the variable insertion domain between motifs 2 and 3. The main features of the catalytic domain are the active site cavity formed upon the surface of a six-stranded antiparallel β-sheet and notably comprising motifs 2 and 3, and the dimer interface which includes

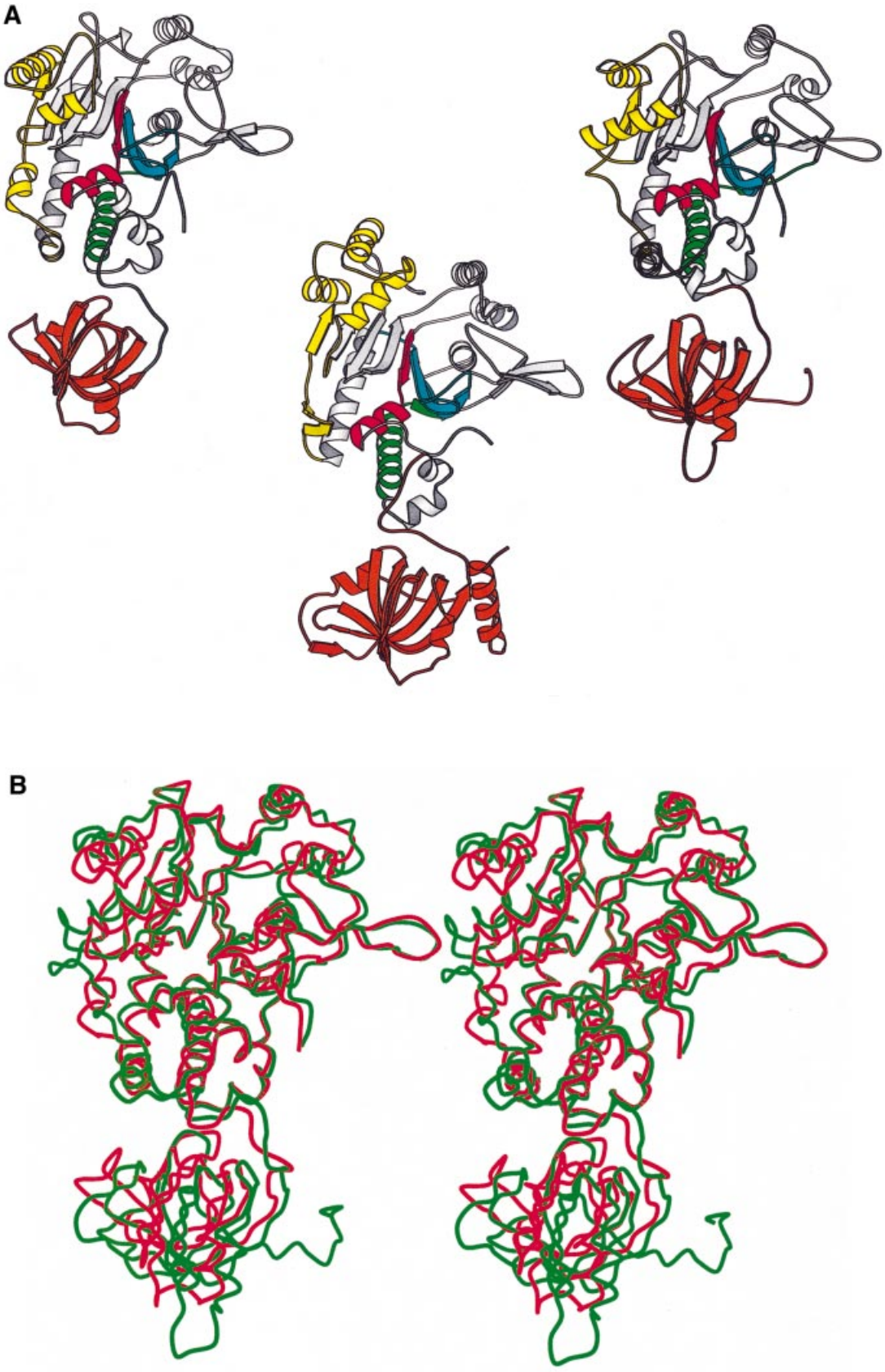


**Fig. 3.** Comparison of structures of class IIb synthetases. (**A**) Ribbon diagrams showing single subunits of the three class IIb aminoacyl-tRNA synthetases. Left, *T.thermophilus* asparaginyl-tRNA synthetase; centre, *T.thermophilus* lysyl-tRNA synthetase (Cusack *et al*., 1996); right, yeast aspartyl-tRNA synthetase (Ruff *et al*., 1991). The class II-specific motifs in the catalytic domain are shown in green (motif 1), blue (motif 2) and red (motif 3). The sub-class conserved N-terminal anticodon-binding domain is orange. System conserved domains are of variable size and tertiary fold (yellow). (**B**) Superposition of Cα traces of AsnRSTT (red) and AspRSSC (green). Note the relative rotation of the N-terminal β-barrel domain.

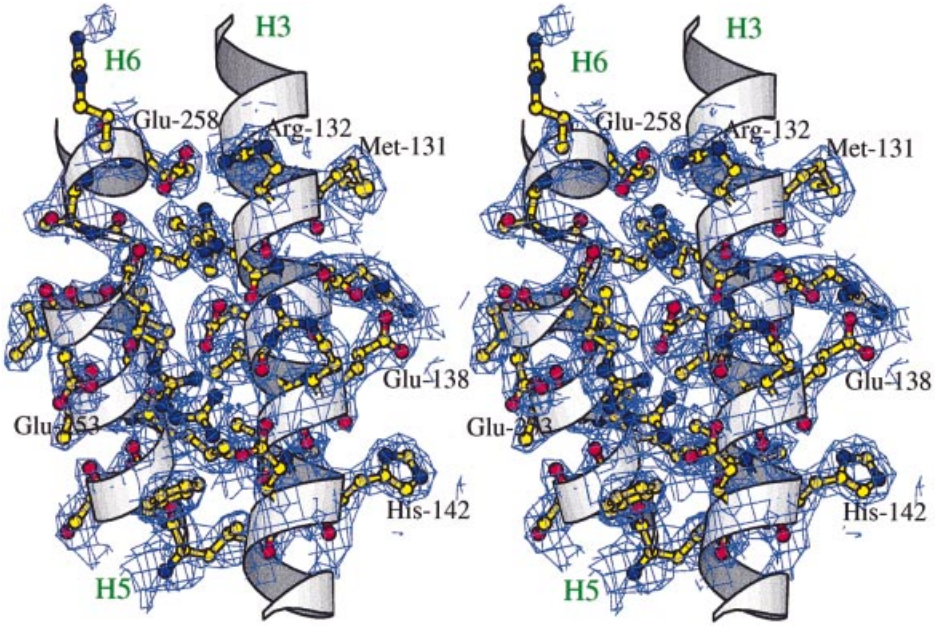


**Fig. 4.** Extensive salt bridge network between charged residues from helices H3, H5 and H6 (see text). The superposed density is the final sigma-weighted $2F_o–F_c$ map from the refined uranium derivative model contoured at 1.2σ.

the conserved motif 1. The insertion domain extends from residue 256 to 318 and contains the four α-helices H6, H7, H8 and H9 and the β-strand A4 which is between H7 and H8 and forms an extra strand parallel to the conserved six-stranded antiparallel β-sheet of the catalytic domain. The topology of the insertion domain is similar to that of yeast aspartyl-tRNA synthetase, whereas that of the prokaryotic aspartyl-tRNA synthetases such as AspRSTT and AspRSEC is a much larger structure (Delarue *et al*., 1994; Poterszman *et al.*, 1994). This reflects the previously noted closer similarity between asparaginyl-tRNA synthetases and eukaryotic rather than prokaryotic aspartyl-tRNA synthetases. As shown in Figure 4, an interesting feature of the C-terminal domain surface is an extensive intra-subunit cluster of interacting charged residues involving Arg132 (Arg), Asp135 (His), Glu136 (Thr), Arg139 (Gln) and Glu143 (Arg) from the interface helix H3, and Arg250 (Ala), Glu253 (Glu), Arg254 (Glu), Arg255 (Arg) and Glu258 (Asp) from the helices H5 and H6 (AsnRSEC equivalent residues in parentheses). This kind of extended ion pair cluster has been found in many thermophilic enzymes and is hypothesized to be a means of thermal stabilization (Yip *et al*., 1995).

### *The dimer interface*

In common with other class II synthetases, an important part of the dimer interface consists of inter-C-terminal domain contacts mediated by the conserved motif 1 which is made up of a long α-helix H3 (125–147) followed by an extended strand (151–159). The helix (H3) runs antiparallel to the 2-fold-related helix H3′ of the second monomer at the 'top' of the dimer interface. Inter-subunit interactions between the interface helices H3 and H3′ and following strands A1 and A1′ are generally polar, with Arg134, Asp135, Glu138, Arg152 and Asp154 (and their symmetry equivalents) being involved. His142 stacks against its symmetry equivalent about the dimer 2-fold axis. In addition, on the 'bottom' of the molecule, the β-strands I1 (171–173) and I2 (179–182) from one monomer constitute an antiparallel β-sheet with the symmetrically related strands I1 and I2 from the second monomer, reinforcing the dimerization interface. As in other class II synthetases, the poorly ordered loops between I1 and I2 (175–178) cross over to be close to the active site of the other subunit. The internal part of the dimer interface is largely hydrophobic, comprising Ile157, Leu158, Phe170, Val172, Leu174 and Leu182 of strands A1, I1 and I2 together with Phe207 of motif 2 (and their symmetry equivalents). This hydrophobic core as well as the hydrogen bonds between the side chain of Glu220 and the peptide oxygens of Ile157 and Leu158 intimately link the ATP-binding site with the dimer interface, and the conserved motif 1 Pro156 (e.g. Arg208 and Phe221 interact directly with the ATP; Figure 6B), as previously described for yeast aspartyl-tRNA synthetase (Eriani *et al*., 1993).

There are also important inter-subunit contacts between the C-terminal domain of one subunit and the N-terminal and hinge domains of the other subunit. These are considered in the Discussion in the context of propagation of substrate-induced conformational changes.

### *ATP binding*

The structure of the complex of asparaginyl-tRNA synthetase with its substrate ATP-$Mg^{2+}$ has been determined at 2.95 Å resolution. Soaking in ATP-$Mg^{2+}$ solution induces an initial disordering of the $P6_422$ crystal form and results, after a few hours, in a new $P6_522$ hexagonal space group in which the dimer becomes the asymmetric unit. Examination of this structure reveals that the two subunits have only minor differences which seem to be related to resolution of conformational disorder by symmetry breaking, e.g. Glu234 in the $P6_422$ has double occupation, observed separately in each distinct subunit in $P6_522$. The occurrence of the $P6_522$ form is not reproducible (e.g. with ATP-$Mn^{2+}$ soaks it has not been observed) and may in fact be a transient stage, trapable by cryo-cooling,

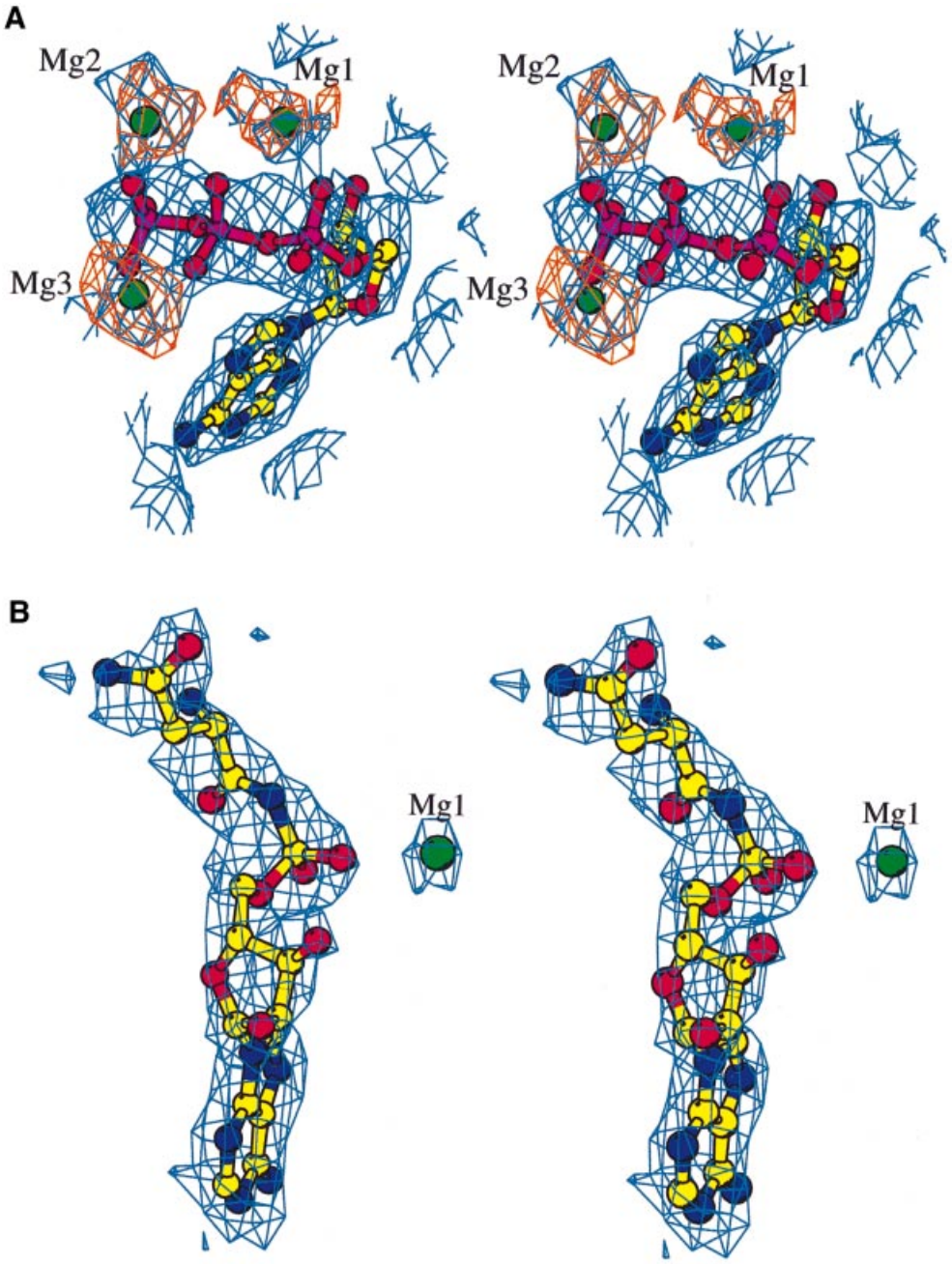


**Fig. 5.** Stereo diagrams showing experimental electron density for the substrates. (**A**) Sigma-weighted $2F_o–F_c$ electron density for the ATP (royal blue, contoured at 1.1) before the inclusion of magnesium ions in the refinement which appear as strong positive peaks (>4.5) in the difference density (orange, contoured at 3.3σ). (**B**) Unbiased positive difference density for the asparaginyl-adenylate analogue (Asn-AMS) and its associated magnesium ion contoured at 3σ.

before reversion to the $P6_422$ form when the ATP site is essentially fully occupied in each subunit. However, the observation may indicate some intrinsic asymmetry in the enzyme with respect to ATP binding as has been invoked previously for aspartyl-tRNA synthetase (Eriani *et al*., 1993).

Despite the relatively modest resolution of the data, the mode of binding of the ATP is clearly observed (Figure 5A) and found to be very similar to that occurring in other class II enzymes with the expected roles of the highly conserved motif 2 and 3 residues confirmed (Figure 6A). The superposition of unliganded asparaginyl-tRNA synthetase and its complex with ATP shows no major changes in structure except for the ordering of the motif 2 loop (residues 210–217) as previously documented for other class II enzymes (Cavarelli *et al*., 1993; Belrhali *et al*., 1995). The loop is ordered into a β-hairpin structure as a result of interactions with the pyrimidine moiety of the ATP (notably the main chain of Leu218 with the N6 and N1) and with Arg216 and His217 which hydrogen-bond to the γ-phosphate (Figure 6A). This stabilizes the ATP in the characteristic bent conformation previously described in other class II synthetases and which is essential for the in-line displacement mechanism for the amino acid activation (Cavarelli *et al*., 1993; Belrhali *et al*., 1995). Of particular interest is the observation of well-defined electron density for three putative magnesium ions associated with the triphosphate (Figure 5A), one

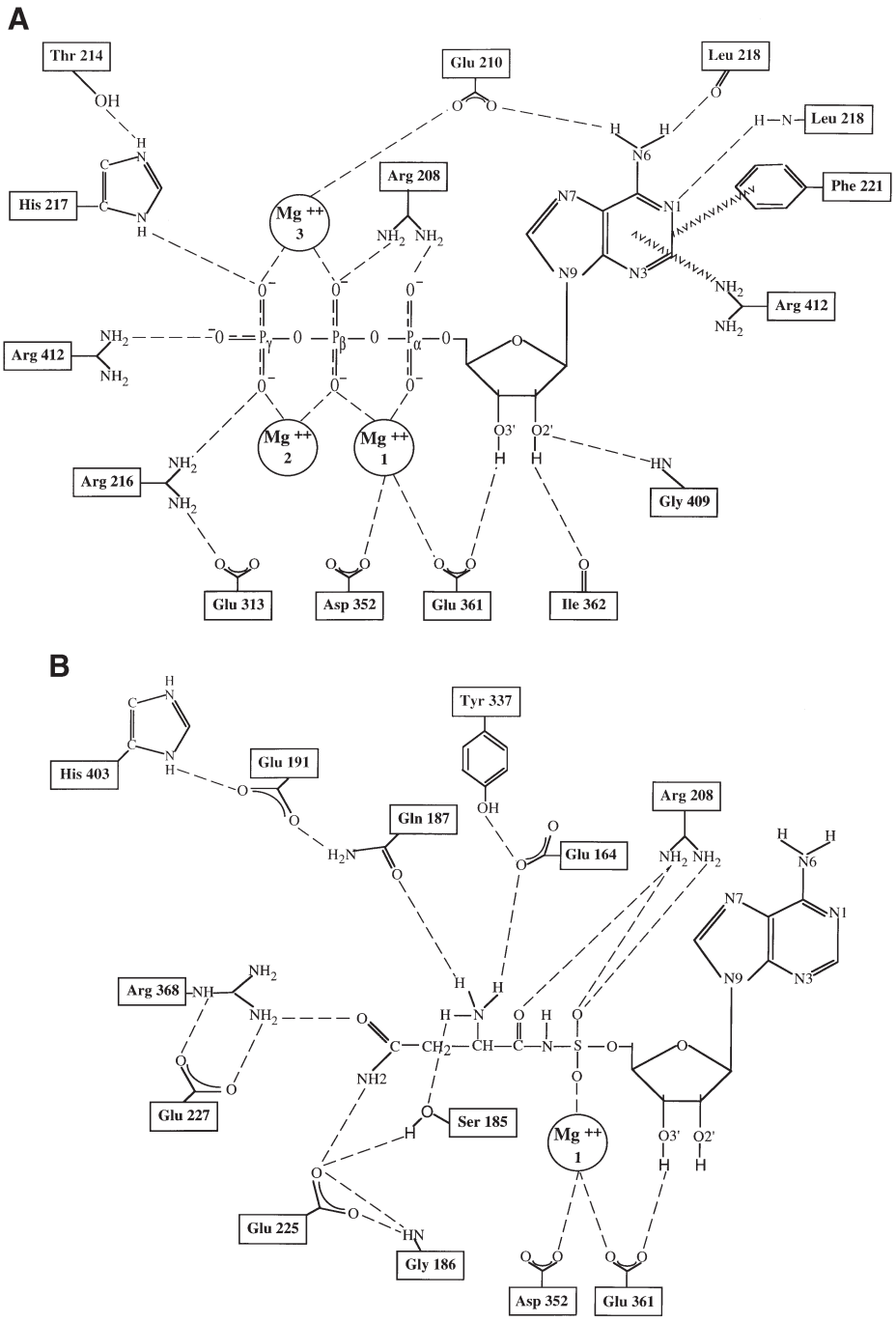


**Fig. 6.** Interactions with the substrates. Hydrogen bonds (<3.5 Å) are indicated by dotted lines, direct magnesium ions by double dotted lines, and stacking interactions by wavy lines. (**A**) Interactions between the ATP and three associated magnesium ions and the active site residues. (**B**) Interactions between the Asn-AMS and one associated magnesium ion and the active site residues. Interactions with the base and ribose of Asn-AMS are as in (A).

between the α- and β-phosphates (Mg-1) and one each side of the β–γ phosphate linkage (Mg-2 and Mg-3). The identity of these ions has been partially confirmed by a 3.5 Å data collection with ATP-$Mn^{2+}$-soaked crystals which revealed a clear anomalous signal at the Mg-1 position, but not at the other positions, probably due to poor data quality. However, since the three ions are in exactly the same configuration as the three divalent ions described in the seryl-tRNA synthethase complex with ATP (Belrhali *et al.*, 1995), we are confident of their assignment. Two of the enzyme ligands of Mg-1 are conserved in essentially all class II synthetases, Glu361 (Glu343 in SerRSTT) and Asp352 (Asp332 in SerRSTT, a water-mediated interaction), the third observed in SerRSTT, Ser348, is not present in AsnRSTT due to its replacement by a glycine. The clear observation in AsnRSTT of magnesium ions associated with the ATP (and with the asparaginyl-adenylate, see below), despite the modest resolution, is probably due to the relatively low salt concentration in the crystallization medium (0.3 M KCl). In the studies on SerRSTT, competition with sulfate ions from the crystallization medium prevented correct

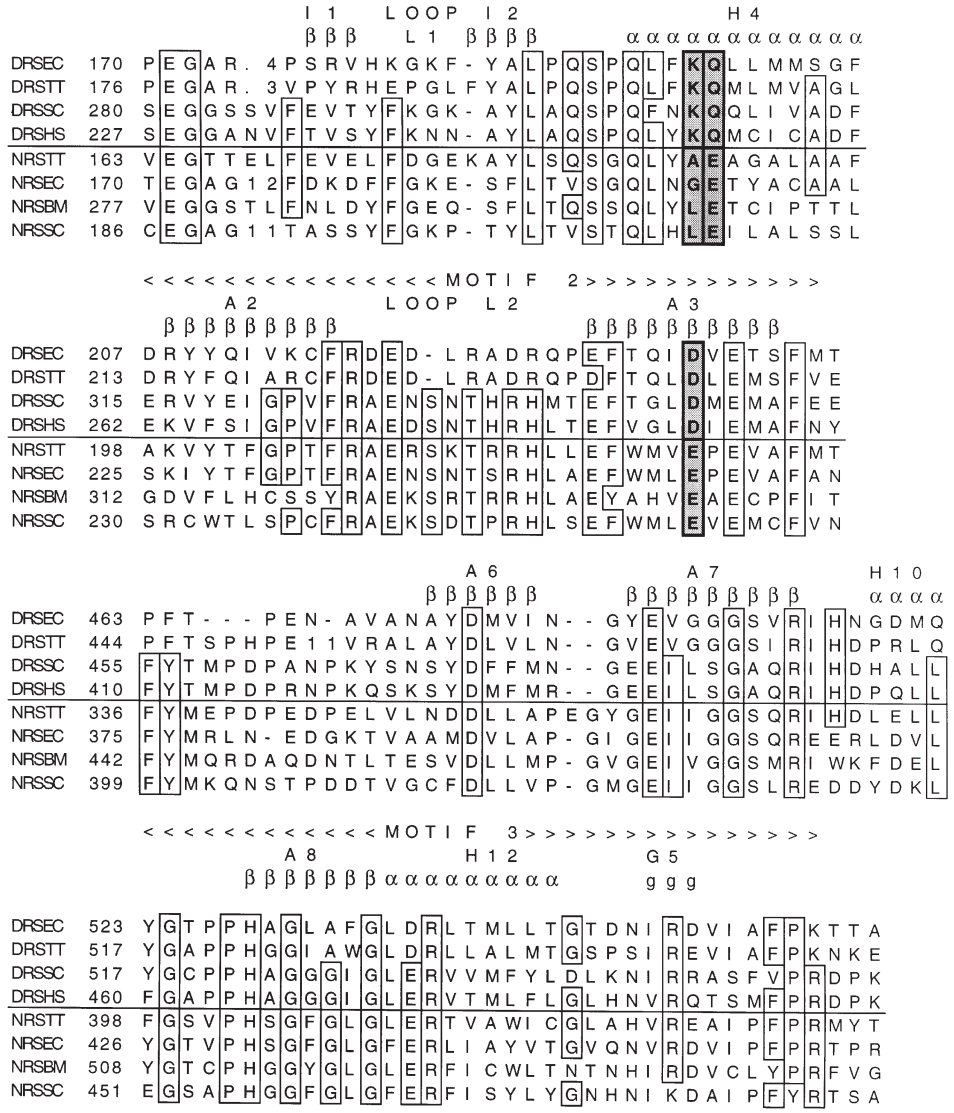

**Fig. 7.** Comparison of sequences of four asparaginyl-tRNA synthetases (NRSXX) and four aspartyl-tRNA synthetases (DRSXX) in four regions contributing important active site residues. Boxes indicate highly conserved residues occurring in both enzymes. The yellow boxes indicate the three key systematic differences between the two enzymes (see text and Table I). Abbreviations for organisms (XX) are as in Table I.

binding of the ATP phosphates except in the presence of manganese (Belrhali *et al.*, 1995). We also point out that the distinct trivalent samarium site observed in AsnRSTT is formed by Glu361, Asp352 and Glu313 and is displaced ~4 Å from the Mg-1 site. The confusion of these sites has led to uncertainty about the true magnesium binding-sites in aspartyl-tRNA synthetase (Cavarelli *et al.*, 1993; Poterszman *et al.*, 1994; Belrhali *et al.*, 1995). Recent results on glycyl-tRNA synthetase and archae aspartyl-tRNA synthetase (D.Moras, personal communication), however, support the conclusion that three divalent cation sites associated with ATP occur in all class II synthetases, except histidyl-tRNA synthetase where a specific additional arginine plays the role of Mg-1 (Åberg *et al.*, 1997; Arnez *et al.*, 1997; Cusack, 1997). These results based on crystallographic analysis are consistent with an independent study of the magnesium dependence of ATP/PPi exchange and aminoacylation reactions of three class I and three class II *E.coli* aminoacyl-tRNA synthetases. This confirmed that the magnesium dependence of class I and class II synthetases is distinct, one magnesium being required for class I and three for the class II enzymes (Airas, 1996).

### *Asparaginyl-tRNA synthetase crystals containing asparaginyl-adenylate or the inhibitor Asn-AMS*

The electron density map at 3.2 Å resolution obtained from crystals co-crystallized with the ATP-$Mg^{2+}$ and L-asparagine shows by the clear presence of the asparaginyl-adenylate bound in the active site (difference map not shown) that the activation reaction has occurred. The conformation of the adenylate is elongated as in the other class II synthetases, and a putative magnesium ion is clearly visible in the Mg-1 site (as has also been observed in the case of seryl-adenylate, Belrhali *et al.*, 1995). The quality of the electron density map at 2.65 Å resolution obtained from crystals containing the inhibitor 5′-*O*-(*N*-asparaginyl-sulfamoyl)adenosine (Asn-AMS) was much better (Figure 5B). This permits a clearer definition of the interactions between the active site residues and the

**Table I.** Equivalent active site residues in asparaginyl- and aspartyl-tRNA synthetases

| | | AsnRSTT | AspRSTT | AspRSSC[a] | Principal interaction |
|---|---|---|---|---|---|
| ATP | 1 | Arg208 | Arg223 | Arg325 | α-phosphate |
| | 2 | Glu210 | Glu225 | Glu327 | base N6 |
| | 3 | His217 | Arg231 | His333 | γ-phosphate |
| | 4 | Leu218 | Gln232 | Met334 | main chain to base |
| | 5 | Phe221 | Phe235 | Phe337 | stacks with base |
| | 6 | Arg412 | Arg431 | Arg531 | γ-phosphate/base |
| Magnesium | 7 | Asp352 | Asp469 | Asp471 | Mg-1 ($H_2O$ mediated) |
| | 8 | Glu361 | Glu476 | Glu478 | Mg-1, Mg-2 |
| Samarium | 9 | Glu313 | – | Glu427 | with (7) and (8) |
| Amino acid | 10 | Glu164 | Glu177 | Glu281[a] | α-amino group |
| | 11 | Ser185 | Ser199 | Ser301[a] | α-amino group |
| | 12 | Gln187 | Gln201 | Gln303 | α-amino group (not AspRS) |
| | 13 | Ala190 | Lys204 | Lys306 | amino acid side chain (not AsnRS) |
| | 14 | Glu191 | Gln205 | Gln307 | H-bonds with (12) and (18) |
| | 15 | Glu225 | Asp239 | Asp342 | $NH_2$ of asparagine Lys (13) in AspRS |
| | 16 | Glu227 | Glu241 | Glu344 | stabilizes (17) |
| | 17 | Arg368 | Arg483 | Arg485 | amino acid side chain |
| | 18 | His403 | His522 | His522 | donor to (14) |

[a]In AspRSSC, only structures in the presence of tRNA are available, in which case certain residues such as Glu281 and Ser301 are found interacting with Ade76 of the tRNA rather than with the amino acid substrate (Cavarelli *et al*., 1994).

asparaginyl-adenylate analogue. The results are consistent with that found for the asparaginyl-adenylate–$Mg^{2+}$ complex, including the presence of the magnesium in the Mg-1 site. Figure 6B shows a schematic diagram of the interactions between the inhibitor and the enzyme. The interactions with the adenosine moiety are similar to those observed in the ATP complex. The α-amino group of the asparagine moiety is positioned by the side chains of three residues, Glu164, Ser185 and Gln187. Of these residues, Glu164 is part of a flexible loop (residues 161–168) which is disordered in the absence of the asparagine substrate. The asparagine side chain carbonyl group makes one hydrogen bond with Arg368 which is conserved in the aspartyl-tRNA synthetase (Arg485 in AspRSSC) and essential for the recognition of aspartic acid (Cavarelli *et al*., 1994). The amide group of the side chain makes a hydrogen bond with the carboxyl side chain of Glu225. These results are discussed with reference to discrimination against aspartic acid below.

## Discussion

The three members of the class IIb aminoacyl-tRNA synthetases are, from their primary and tertiary structures, clearly a closely homologous set of enzymes (Figure 3A and B). The goals of structural studies of them are therefore centered around identifying the characteristics which ensure their specificity in recognizing cognate amino acids and tRNAs. Since this group of enzymes contains the aspartyl- and asparaginyl-tRNA synthetases, one main interest in the structure determination of the latter is to define the preferential mode of interaction of asparagine with the enzyme against interaction with aspartate.

The active sites of the yeast or *T.thermophilus* aspartyl- and *T.thermophilus* asparaginyl-tRNA synthetases are astonishingly similar. As highlighted in Figure 7 and Table I, most active site residues in close proximity to the ATP or amino acid substrates are identical except for three systematic differences between all asparaginyl- and aspartyl-tRNA synthetases: (i) a lysine absolutely conserved in aspartyl-tRNA synthetases (Lys204 in AspRSTT) is replaced by small or uncharged residue in all asparaginyl-tRNA synthetases (Ala190 in AsnRSTT); (ii) the following residue is invariably a glutamine in aspartyl-tRNA synthetases (Gln205 in AspRSTT) and glutamic acid in asparaginyl-tRNA synthetases (Glu191 in AsnRSTT); and (iii) in motif 2, there is an invariant aspartic acid in aspartyl-tRNA synthetases (Asp239 in AspRSTT) and a glutamic acid in asparaginyl-tRNA synthetases (Glu225 in AsnRSTT). There are other residue differences between AsnRSTT and AspRSTT close to the amino acid substrate, notably the substitution of Tyr337 by Phe445 in AspRSTT (Figures 7 and 8) and the presence of His442 and His443 in AspRSTT, His442 providing an additional hydrogen bond to the substrate aspartic acid side chain (Poterszman *et al*., 1994). However, these differences are species specific and, although significant, are not discussed further here.

Figure 8A and B compares the interactions with the amino acid moiety of the adenylate for AsnRSTT and AspRSTT (Poterszman *et al*., 1994) and shows the structural basis for distinguishing between the carboxyl and amide side chains of the respective amino acid substrates of the two enzymes. The key to the recognition of aspartic acid by aspartyl-tRNA synthetase is the electrostatic complementarity between the substrate side chain carboxylate group and the guanidinium group of Arg483 (with which two hydrogen bonds are made) and Lys204 (AspRSTT numbering) which are in turn positioned by Glu241 and Asp239. This would clearly be an unfavourable environment for an asparagine held in the same orientation. In AsnRSTT, residues Arg368 and Glu227 have exactly the same configuration as Arg483 and Glu241 in AspRSTT, but the unfavourable head-on interaction between the asparagine carboxyamide and Arg368 is avoided by a 60° rotation about the substrate C–Cα bond which turns the side chain more into the active site (Figure 8A). This not only enables retention of one hydrogen bond between the carbonyl oxygen of the side chain and

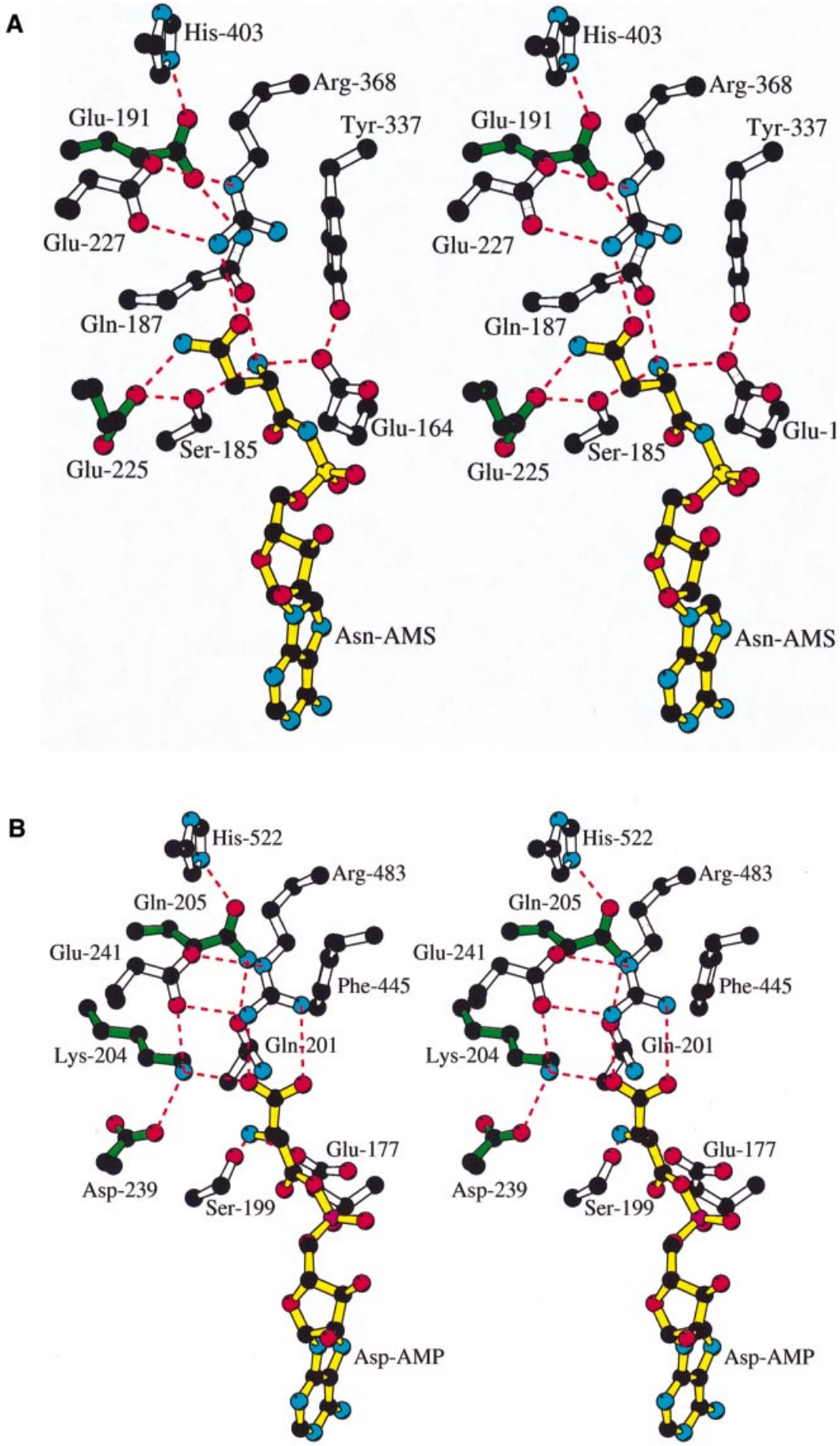


**Fig. 8.** Stereo diagrams comparing the interactions of the amino acid moiety of the adenylate for (**A**) AsnRSTT and (**B**) AspRSTT (Poterszman *et al*., 1994). Residues which are systematically different between the two enzymes are shown in green. Hydrogen bonds are shown by red dotted lines.

**Table II.** Data collection and phasing statistics

**Structure solution**

| | AsnRS Native | SmNO3 | Uacetate |
|---|---|---|---|
| Beamline | BM14 | BM14 | BM14 |
| Detector | 300 mm Mar | 300 mm Mar | 300 mm Mar |
| Wavelength | 0.93 Å | 0.93 Å | 0.88 Å |
| Exposure/image | 120 s/1° | 120 s/0.8° | 150 s/1° |
| No. of crystals | 1 (frozen) | 1 (frozen) | 1 (frozen) |
| Resolution | 31–2.8 Å | 31–2.8 Å | 43–2.6 Å |
| Total reflections | 73 000 | 160 045 | 70 630 |
| Unique reflections | 14 619 | 14 864 | 17 567 |
| Average redundancy | 5.0 | 10.8 | 4.0 |
| Completeness | 98.9 | 100 | 96.3 |
| *R*-merge (highest bin) | 0.067 (0.250) | 0.065 (0.157) | 0.033 (0.075) |
| **Heavy-atom refinement and phasing** | | | |
| Resolution used | 2.85 Å | 4 Å | 2.85 Å |
| No. of sites | | 1 | 2 |
| Phasing power | | 1.33 | 1.70 |
| *R*-cullis | | 0.74 | 0.68 |
| Mean figure of merit | | | |
| acentric | 0.409 | | |
| centric | 0.631 | | |
| all | 0.444 | | |

**Substrate complexes**

| | Asn-adenylate | AsnRS + Asn-AMS | AsnRS-ATP |
|---|---|---|---|
| Beamline | BM14 | BM14 | Swiss–Norwegian |
| Detector | 300 mm Mar | 300 mm Mar | 300 mm Mar |
| Wavelength | 1.002 Å | 0.890 Å | 0.87 Å |
| Exposure/image | 360 s/1° | 160 s/1° | 360 s/0.8° |
| Space group | $P6_422$ | $P6_422$ | $P6_522$ |
| No. of crystals | 1 (frozen) | 1 (frozen) | 1 (frozen) |
| Resolution | 27–3.2 Å | 15–2.62 Å | 24–2.95 Å |
| Total reflections | 46 376 | 120 269 | 168 818 |
| Unique reflections | 9777 | 16 965 | 23 382 |
| Average redundancy | 4.7 | 7.1 | 7.2 |
| Completeness | 99.8 | 94.5 | 94.5 |
| *R*-merge (highest bin) | 0.081 (0.27) | 0.052 (0.262) | 0.105 (0.271) |

Arg368, but also permits a hydrogen bond between an amide hydrogen and Glu225. The asparaginyl-tRNA synthetase-specific Glu225 has, therefore, the dual role of positive recognition of asparagine and discrimination against the negatively charged aspartic acid side chain. Lys204 in aspartyl-tRNA synthetase fulfils the inverse dual role with respect to substrate discrimination. In aspartyl-tRNA synthetase, the equivalent residue to Glu225 is the shorter Asp239 which helps position the aspartyl-tRNA synthetase-specific Lys204 but is itself too distant from the aspartic acid side chain to make an unfavourable electrostatic interaction. It should be noted that the interactions described so far would not permit discrimination by asparaginyl-tRNA synthetase between asparagine and protonated aspartic acid. This would necessitate specific recognition of both amide hydrogens of the asparagine and could be achieved, for instance, by a water molecule, except that in the current structure none are visible in the required position.

As mentioned above, the rotation of the substrate side chain is a crucial difference between cognate amino acid binding to asparaginyl- and aspartyl-tRNA synthetase. How is this achieved? The rotation implies a displacement of the position of the α-amino group of the amino acid. In AsnRSTT, the α-amino group is positioned precisely by three hydrogen bonds with conserved residues Ser185, Gln187 and Glu164. The last residue is on a flexible loop (residues 161–168) which is disordered in the absence of the amino acid substrate. In AspRSTT, these three residues are identical (Ser199, Gln201 and Glu177, respectively), but subtle changes in the exact position of side chains result in the required different position of the α-amino group of the aspartic acid. This is partly explained by the systematic difference between structurally equivalent residues Gln205 and Glu191 in respectively AspRSTT and AsnRSTT. These residues, themselves orientated unambiguously by hydrogen bonds to a conserved motif 3 histidine (His522 and His403 in AspRSTT and AsnRSTT, respectively), hydrogen-bond with equivalent residues Gln201 and Gln187 in AspRSTT and AsnRSTT, respectively. This implies a reversal in the positions of the hydrogen bond acceptor and donor atoms of the carboxyamide group of these two glutamines. Whereas the carbonyl oxygen of Gln187 in AsnRSTT is orientated correctly to accept a hydrogen bond from the α-amino group of asparagine, this is not the case in AspRSTT where Gln201 appears to donate a hydrogen bond to the aspartic acid side chain (Poterszman *et al*., 1994). The conclusion of this discussion is that whereas mutagenesis of the three systematically different residues between aspartyl- and asparaginyl-tRNA synthetase would leave the two active sites virtually identical, it is still questionable whether this would lead to a switch in amino acid specificity, since even the position of identical side chains can be influenced subtly by remaining differences further away.

The binding of the activated intermediate, the asparaginyl-adenylate, in the active site leads to local changes in the active site as well as small but significant concerted changes in the enzyme tertiary and quarternary structure, which do not occur when only ATP is bound. These become apparent after comparing the structure of the native enzyme with that complexed with the adenylate after superposition of helix H3 and the β-sheet formed by I1 and I2, the principal elements of the dimer interface. The principal changes in the vicinity of the active site are the ordering of both the motif 2 loop and the loop preceding I1 (161–168) which swings over the entrance of the active site as if closing 'the door' in order to retain the activated substrate. The ordered conformation of this loop is stabilized by new interactions between Glu164 and both the asparagine α-amino group and Tyr337 (Figure 8A), between Gln184 and the main chain amides of residues 163–164, and between Ala162 and Ser161 and residues Tyr389 and Trp391 on helix H11. The latter draw the helices H10 and H11 (which form a rigid unit held together by inter-helical interactions on one side of the active site) slightly towards the active site which, in turn, induces a movement of the N-terminal β-barrel relative to the catalytic domain by ~2.5° by virtue of inter-subunit interactions between residues of H10 and the N-terminal and hinge domain of the other subunit (denoted *) (Asp394 with His119*, Arg397 with Gln99*, Phe398 with Arg123*, Gly399 with Trp21* and Glu66*, and Ser400 with Ser96*). On the other side of the active site from H10 and H11, the motif 2 loop and the C-terminal peptide move in a concerted way towards the active site. A similar mechanism for conformational change and relative domain move-

**Table III.** Summary of refinement

| | AsnRS-U | AsnRS + ATP | AsnRS + AsnAMS |
|---|---|---|---|
| Resolution (Å) | 12–2.6 | 12–2.95 | 15–2.65 |
| Cell dimensions (Å) | $a = b = 124.4$, $c = 123.4$ | $a = b = 124.9$, $c = 246.8$ | $a = b = 125.2$, $c = 126.6$ |
| Solvent content | 55.5% | 54.6% | 54.6% |
| Work reflections | 16 667 | 22 135 | 16 084 |
| Test reflections | 900 (5.1%) | 1185 (5.1%) | 872 (5.1%) |
| *R*-free | 0.253 | 0.254 | 0.303 |
| *R*-work | 0.207 | 0.220 | 0.226 |
| No. of protein atoms (occ>0) | 3457 | 7090 | 3593 |
| No. of substrate atoms | – | 62 (ATP) | 31 (Asn-AMS) |
| No. of water molecules | 65 | 5 | 10 |
| No. of metal atoms | 2×U | 6×Mg | 1×Mg |
| <b> protein | 36.9 | 44.0 | 52.7 |
| <b> solvent | 28.1 | 23.4 | 48.0 |
| <b> substrate | – | 40.3 | 45.9 |
| R.m.s. bonds (Å) | 0.005 | 0.005 | 0.006 |
| R.m.s. angles (°) | 1.228 | 1.203 | 1.288 |
| Ramachandran plot | | | |
| % favourable | 91.3% | 88.9% | 84% |
| % additional | 8.5% | 10.4% | 15.5% |
| No. generous | 0 | 3 (poorly ordered) | 1 |
| No. disallowed | 1 (Ala198) | 2 (2×Ala198) | 1 (Ala198) |

ment has been described in the other class IIb synthetases, *T.thermophilus* aspartyl-tRNA synthetase (Delarue *et al*., 1994) and lysyl-tRNA synthetase, where in particular, lysine binding has been shown to induce significant tertiary rearrangements (Cusack *et al*., 1996; S.Onesti *et al*., personal communication).

It should be recalled that not all organisms contain an asparaginyl-tRNA synthetase. For example, a gene for this enzyme has not been identified in the genomes of *Methanococcus jannaschii* (Bult *et al*., 1996) or *Helicobacter pylori* (Tomb *et al*., 1997). It is likely that in these organisms $tRNA^{Asn}$ is first aspartylated and the bound aspartate is then amidated, a pathway that has been demonstrated in the case of *Haloferax volcanii* (Curnow *et al*., 1996) and analogous to that found for the glutaminyl system in several organisms (reviewed in Ibba *et al*., 1997). From this observation, it seems likely that the very close similarity between asparaginyl-tRNA synthetase and especially eukaryotic aspartyl-tRNA synthetase is a result of the relatively recent evolution of the former from the latter as an alternative to the original transamidation pathway of asparaginylation. Interestingly, there is a third enzyme which is clearly closely related in evolution to these two synthetases. This is the ammonia-dependent asparagine synthetase, which converts aspartic acid into asparagine via an ATP-activated intermediate using ammonia as the amide source. A significant difference is that in AspRS the aspartyl-adenylate is made with the α-carboxyl-group whereas in the asparagine synthetase it is made with the β-carboxyl-group. The mechanistic similarity and primary sequence homology to aspartyl-tRNA synthetase was first noted by Gatti and Tzagoloff (1991). The recent crystal structure of this enzyme together with its product complex (AMP and asparagine) shows that its tertiary structure indeed resembles very closely that of yeast aspartyl-tRNA synthetase. The only two essential differences in the active site are responsible for the binding of the substrate aspartic acid in the reverse sense (Nakatsu *et al*., 1998).

## Materials and methods

### *Synthesis of 5′-O-[N-(L-asparagine)sulfamoyl]adenosine*

5′-*O*-[*N*-(L-asparagine)sulfamoyl]adenosine was synthesized by a procedure analogous to that described for the corresponding alanyl (Ueda *et al*., 1991) and seryl (Belrhali *et al*., 1994) compounds. 2′,3′-*O*-Isopropylidene-5′-*O*-sulfamoyladenosine was reacted with *tert*-butyloxycarbonyl-L-asparagine *N*-hydroxysuccinimide ester and 1,8-diazabicyclo-[5,4-0]undec-7-ene in anhydrous dimethylformamide under argon for 4 h at room temperature. The product, 2′,3′-*O*-isopropylidene-5′-*O*-[*N*-(BOC-L-asparagine)sulfamoyl]adenosine, was purified by column chromatography on fluorosil gel by elution with a gradient of 0–15% ethanol in dichloromethane. The pure product was obtained as a white solid product in 79% yield. This material was then treated with trifluoroacetic acid/water (2:1 v/v) at room temperature for 2 h to remove the butyloxycarbonyl protecting groups. The solvent was then removed by distillation *in vacuo*, the residue dissolved in methanol and the product precipitated by slow addition under stirring of diethylether. The product was recovered by filtration, washed with diethylether and dried under vacuum.

### *Crystallization and data collection on native crystals*

Crystals of *T.thermophilus* asparaginyl-tRNA synthetase were grown from purified protein expressed in *E.coli* as described by Seignovert *et al*. (1996). Crystallization trials led to two different crystal forms growing under very similar conditions but identifiable by their distinctive habits (Berthet-Colominas *et al*., 1997). The tetragonal form of space group $P4_32_12$ (#96) has unit cell dimensions of $a = b = 83.9$ Å, $c = 167.9$ Å, $\alpha = \beta = \gamma = 90°$ and diffract to 3 Å resolution. Crystals belonging to $P6_422$ (#181) have a unit cell of $a = b = 124.7$ Å, $c = 122.6$ Å, $\alpha = \beta = 90°$, $\gamma = 120°$ and diffract to 2.6 Å resolution. A third crystal form belonging to the space group $P3_121$ was only obtained in the presence of mercuric nitrate (C.Berthet-Colominas and X.Huot, unpublished results). In all these space groups, the asymmetric unit is the monomer, the dimer axis coinciding with a crystallographic 2-fold axis. Data were collected at 100 K on both crystal forms using synchrotron radiation (Table II). The crystals were cryo-protected by transfering in five steps to mother liquor containing 30% glycerol. Data were integrated with MOSFLM (Leslie, 1992) and subsequent data processing was done with the CCP4 package (1994).

### *Data collection on derivatives*

Two isomorphous derivatives were obtained by soaking hexagonal crystals with mother liquor containing 2 mM samarium nitrate hexahydrate or 10 mM uranyl nitrate. Data were collected at 100 K to 2.8 and 2.6 Å resolution, respectively, on BM14 at the ESRF (Table II). A characteristic of the hexagonal crystal form was the stability in the

length of the $a = b$ axes, on the other hand the *c*-axis varies slightly when a change is induced in the crystal (derivatives or complexes).

### Crystals and data collection on substrate complexes

*Crystals containing ATP.* When native hexagonal crystals were soaked in mother liquor containing 5 mM ATP and 10 mM $MgCl_2$, parallel striations perpendicular to the *c*-axis appeared. After several hours of soaking, the crystals recovered their initial aspect. Data on these crystals at 100 K were collected using the Swiss–Norwegian beam line (BM1) at the ESRF (Table II). Soaking with ATP induced a change in the space group to $P6_522$ (#179, determined by molecular replacement) with unit cell dimensions $a = b = 124.7$ Å, $c = 246.82$ Å, $\alpha = \beta = 90°$, $\gamma = 120°$. The *c*-axis is thus doubled and the enzyme dimer axis becomes non-crystallographic, although the crystal packing is very similar to the $P6_422$ form.

*Crystals containing asparaginyl-adenylate.* Attempts to synthesize asparaginyl-adenylate *in situ* by soaking ATP, $Mg^{2+}$ and asparagine into native crystals were unsuccessful, with the crystals cracking or disintegrating. Co-crystallization yielded crystals that were smaller than native crystals and difficult to manipulate due to fragility under cryo-protectant conditions. The best data set obtained was at 3.2 Å resolution at 100 K on BM14 at the ESRF. The space group is the same as for native hexagonal crystals and the cell dimensions are similar (Table II). Greater success was achieved using the non-hydrolysable analogue of asparagyl-adenylate, Asn-AMS. A data set to 2.65 Å resolution was obtained on BM14 from a native hexagonal crystal soaked for 15 h in mother liquor containing 100 μM Asn-AMS (Table II).

### Structure solution

Initially attempts were made to solve the structure by molecular replacement using the co-ordinates of the yeast aspartyl-tRNA synthetase (Ruff *et al*., 1991), the synthetase of known structure which most homologous to AsnRSTT. Using the program AMoRe (Navaza, 1994), well packing solutions were found for both the tetragonal and hexagonal crystal forms which, despite the relatively low correlation factors, were in fact correct. Rigid-body refinement with XPLOR v3.1 (Brunger, 1992) treating the N- and C-terminal domains separately led to a significant rotation of the N-terminal domain with a corresponding increase of the correlation as described (Berthet-Colominas *et al.*, 1997). Using the molecular replacement phases as well as averaging between the hexagonal and tetragonal crystal forms using the program DMmulti (Cowtan, 1994), some progress could be made in rebuilding the structure, but several regions remained very poorly defined and further progress could not be made without unbiased phase information. The probable reasons for this were a combination of low homology and low solvent content (~55%) so that at the resolution of these initial trials (2.9 Å) the relatively low number of independent reflections did not permit useful refinement.

The structure was therefore solved independently in the hexagonal space group by multiple isomorphous replacement using two heavy atom derivatives, samarium (one site) and uranium (two sites). A lead derivative (tetramethyl lead acetate) was also identified but the lead ions occupied the same sites as the uranium. The samarium and uranium derivatives share a common major site co-ordinated by three carboxylates in the enzyme active site, Glu313, Asp352 and Glu361. The second uranium site is at a crystal contact and is co-ordinated by Glu270 and Glu274 from one subunit and Glu295 from a second crystallographically related subunit (but not one forming a molecular dimer). This reinforced crystal contact may be responsible for the better diffraction quality of the uranium derivative (Table II). The molecular replacement solution facilitated finding the heavy atom sites but was not necessary since Patterson methods were also successful. Heavy atom refinement and phasing was done with MLPHARE, and the phasing statistics are given in Table III. Anomalous differences were used for the uranium derivative. Solvent flattening and two crystal averaging using DM (Cowtan, 1994) and DMmulti only marginally improved the experimental maps probably because of the low solvent content of the crystals (55% in the hexagonal form, 58% in the tetragonal form) and the lack of derivative data in the tetragonal form. Nevertheless, the multiple isomorphous replacement (MIR) map to 2.85 Å resolution was of sufficient quality to allow a complete model of AsnRSTT to be built. The tetragonal form was particularly useful in permitting building of the first 15 N-terminal residues which are less well-ordered in the hexagonal form.

### Refinement

*Native structure.* Refinement was performed with XPLOR v3.1 (Brunger, 1992) using standard procedures, including solvent correction, combined with manual model building. The best model has been obtained by refining the data of the uranium derivative since these extend to 2.6 Å resolution compared with the best native native data of 2.8 Å resolution. The *R*-free factor was used to avoid over-modelling of the data. The *B*-factors were refined individually. Two uranium atoms were added as well as 65 water molecules in $F_o$–$F_c$ difference density $>4\sigma$. The results of the refinement are shown in the Table III and respresentative density shown in Figure 4.

*Complexes with substrates.* The refined model of asparaginyl-tRNA synthetase was used as search model for molecular replacement of the ATP-soaked crystals. A clear solution in space group $P6_522$ with a correlation of 55% was found using the dimer as starting model. The structure was improved initially using rigid-body refinement and positional refinement with tight NCS restraints which gave rise to a map in which two ATP molecules could be placed in strong positive density difference (up to $10\sigma$). In addition, a number of adjustments were made, notably in the region of motif 2 which interacts with the ATP and in regions of clear asymmetry between the two subunits (e.g. Glu234, Arg279 and Arg319, which take up different conformations in the two subunits). After further positional refinement maintaining tight NCS restraints except in very limited regions, five water molecules and six magnesium ions were added and the final *R*-free (*R*) was 25.4% (22.0%) (Table III).

The 3.2 Å resolution data obtained with the crystals co-crystallized with the asparaginyl-adenylate did not permit extensive refinement. Following rigid-body refinement and energy minimization, clear unbiased difference density was observed for a molecule of asparaginyl-adenylate with an associated magnesium ion. However, data obtained with crystals containing the inhibitor Asn-AMS were of better quality, extending to 2.65 Å. The procedure for the refinement was similar to that followed for the other substrate complexes. In the Asn-AMS structure, both the motif 2 loop and the loop 160–168 (except for 165–167) are well defined. Only 10 molecules of water and one magnesium ion have been included in the structure. The *R*-factor (*R*-free) for data between 15 and 2.65 Å was 22.7% (30.3%) with a tightly restrained geometry (r.m.s. bond and angle deviations of 0.006Å and 1.288°, respectively). This structure is less well determined than the other structures due to the higher *B*-factors (Table III).

## Acknowledgements

We thank Valerie Biou (IBS), Vivian Stojanoff (ESRF), Gordon Leonard (ESRF) and Andrew Thompson (EMBL) for assistance on ESRF beamline BM14, and Phil Patterson and Kenneth Knudsen for assistance on the Swiss–Norwegian CRG beamline at the ERSF. We also thank Dino Moras and Arnaud Poterszman for communication of the co-ordinates of the *T.thermophilus* AspRS–aspartyl-adenylate complex. Figures 1, 3, 4, 5 and 8 were prepared with BOBSCRIPT (Esnouf, 1997).

## References

Åberg,A., Yaremchuk,A., Tukalo,M., Rasmussen,B. and Cusack,S. (1997) Crystal structure analysis of activation of histidine by *T.thermophilus* histidyl-tRNA synthetase. *Biochemistry,* **36**, 3084–3094.

Airas,K.R. (1996) Differences in the magnesium dependences of the class I and class II aminoacyl-tRNA synthetases from *E.coli*. *Eur. J. Biochem*., **240**, 223–231.

Arnez,J.G., Augustine,J.G., Moras,D. and Francklyn,C.S. (1997) The first step in aminoacylation at the atomic level in histidyl-tRNA synthetase. *Proc. Natl Acad. Sci. USA*, **94**, 7144–7149.

Beaulande,M., Tarbouriech,N. and Hartlein,M. (1998) Human cytosolic asparaginyl-tRNA synthetase: cDNA sequence, functional expression in *E.coli* and characterisation as human auto-antigen. *Nucleic Acids Res*., **15**, 521–524.

Belrhali,H. *et al*. (1994) Crystal structure at 2.5 Å resolution of seryl-tRNA synthetase complexed with two analogs of seryl-adenylate. *Science*, **263**, 1432–1436.

Belrhali,H., Yaremchuk,A., Tukalo,M., Berthet-Colominas,C., Rasmussen,B., Bosecke,P., Diat,O. and Cusack,S. (1995) The structural basis for seryl-adenylate and Ap4A synthesis by seryl-tRNA synthetase. *Structure*, **3**, 341–352.

Berthet-Colominas,C., Seignovert,L., Cusack,S. and Leberman,R. (1997) Preliminary X-ray diffraction studies on asparaginyl-tRNA synthetase from *Thermus thermophilus*. *Acta Crystallogr*., **D53**, 195–196.

Brunger,T.A. (1992) *X-PLOR Version 3.1*. Yale University Press, New Haven, CT.

Bult,C.J. *et al.* (1996) Complete genome sequence of the methanogenic archaeon, *Methanococcus jannaschii*. *Science*, **273**, 1058–1073.

Cavarelli,J., Rees,B., Ruff,M., Thierry,J.C. and Moras,D. (1993) Yeast tRNA(Asp) recognition by its cognate class II aminoacyl-tRNA synthetase. *Nature*, **362**, 181–184.

Cavarelli,J. *et al.* (1994) The active site of yeast aspartyl-tRNA synthetase: structural and functional aspects of the aminoacylation reaction. *EMBO J.*, **13**, 327–337.

Collaborative Computational Project Number 4 (1994) The CCP4 suite: programs for protein crystallography. *Acta Crystallogr.*, **D50**, 760–763.

Cowtan,K. (1994) In *Joint CCP4 and ESF-EACBM Newsletter on Protein Crystallography*. **31**, 34–38.

Cusack,S. (1995) Eleven down and nine to go. *Nature Struct. Biol.*, **2**, 824–831.

Cusack,S. (1997) Aminoacyl-tRNA synthetases. *Curr. Opin. Struct. Biol.*, **7**, 881–889.

Cusack,S., Berthet-Colominas,C., Hartlein,M., Nassar,N. and Leberman,R. (1990) A second class of synthetase structure revealed by X-ray analysis of *E.coli* seryl-tRNA synthetase at 2.5 Å resolution. *Nature*, **347**, 249–255.

Cusack,S., Yaremchuk,A. and Tukalo,M. (1996) The crystal structures of *T.thermophilus* lysyl-tRNA synthetase complexed with *E.coli* tRNA(Lys) and a *T.thermophilus* tRNA(Lys) transcript: anticodon recognition and conformational changes upon binding of a lysyl-adenylate analogue. *EMBO J.*, **15**, 6321–6334.

Curnow,A.W., Ibba,M. and Soll,D. (1996) tRNA-dependent asparagine formation. *Nature*, **382**, 589–590.

Delarue,M., Poterszman,A., Nikonov,S., Garber,M., Moras,D. and Thierry,J.C. (1994) Crystal structure of a prokaryotic aspartyl tRNA-synthetase. *EMBO J.*, **13**, 3219–3229.

Esnouf,R.M. (1997) An extensively modified version of MolScript that includes greatly enhanced coloring capabilities. *J. Mol. Graphics*, **15**, 133–138.

Eriani,G., Delarue,M., Poch,O., Gangloff,J. and Moras,D. (1990) Partition of tRNA synthetases into two classes based on mutually exclusive sets of sequence motifs. *Nature*, **347**, 203–206.

Eriani,G., Cavarelli,J., Martin,F., Dirheimer,G., Moras,D. and Gangloff,J. (1993) Role of dimerization in yeast aspartyl-tRNA synthetase and importance of the class II invariant proline. *Proc. Natl Acad. Sci. USA*, **90**, 10816–10820

Gatti,D.L. and Tzagoloff,A. (1991) Structure and evolution of a group of related aminoacyl-tRNA synthetases. *J. Mol. Biol.*, **218**, 557–568.

Hirakata,M., Suwa,A., Kron,M., Nagai,S., Mimori,T., Akizuki,M. and Targoff,I. (1996) Anti-KS: novel autoantibodies to asparaginyl-transfer RNA synthetase. *Arthritis Rheum. Suppl.*, **39**, S39.

Ibba,M., Curnow,A.W. and Soll,D. (1997) Aminoacyl-tRNA synthesis: divergent routes to a common goal. *Trends Biochem. Sci.*, **22**, 39–42.

Kron,M., Marquand,K., Hartlein,M., Price,S. and Leberman,R. (1995) An immunodominant antigen of *Brugia malayi* is an asparaginyl-tRNA synthetase. *FEBS Lett.*, **374**, 122–124.

Laskowski,R.A., MacArthur,M.W., Moss,D.S. and Thornton,J.M. (1993) Procheck: a program to check the stereochemical quality of protein structures. *J. Appl. Crystallogr.*, **26**, 283–291.

Leslie,A.G.W. (1992) In *Joint CCP4 and ESF-EACBM Newsletter on Protein Crystallography*. No. 26, Daresbury Laboratory, Warrington WA4 4AD, UK.

Nakatsu,T., Kato,H. and Oda,J. (1998) Crystal structure of asparagine synthetase reveals a close evolutionary relationship to class II aminoacyl-tRNA synthetase. *Nature Struct. Biol.*, **5**, 15–19.

Navaza,J. (1994) *Acta Crystallogr.*, **A50**, 157–163.

Onesti,S., Miller,A.D. and Brick,P. (1995) The crystal structure of the lysyl-tRNA synthetase (LysU) from *Escherichia coli*. *Structure*, **3**, 163–176.

Poterszman,A., Delarue,M., Thierry,J.-C. and Moras,D. (1994) Synthesis and recognition of aspartyl-adenylate by *T.thermophilus* aspartyl-tRNA synthetase. *J. Mol. Biol.*, **244**, 158–167.

Ruff,M., Krishnaswamy,S., Boeglin,M., Poterszman,A., Mitschler,A., Podjarny,A., Rees,B., Thierry,J.-C. and Moras,D. (1991) Class II aminoacyl transfer RNA synthetases: crystal structure of yeast aspartyl-tRNA synthetase complexed with tRNA(Asp). *Science*, **252**, 1682–1689.

Seignovert,L., Hartlein,M. and Leberman,R. (1996) Asparaginyl-tRNA synthetase from *Thermus thermophilus* HB8; sequence of the gene and crystallization of the enzyme expressed in *Escherichia coli*. *Eur. J. Biochem.*, **239**, 501–508.

Tomb,J.-F. *et al.* (1997) The complete genome sequence of the gastric pathogen *Helicobacter pylori*. *Nature*, **388**, 539–547.

Ueda,H., Shoku,Y., Hayashi,N., Mitsunaga,J., In,Y., Doi,M., Inoue,M. and Ishida,T. (1991) X-ray crystallographic conformational study of 5′-*O*-[*N*-(L-alanyl)-sulfamoyl]adenosine, a substrate analogue for alanyl-tRNA synthetase. *Biochim. Biophys. Acta*, **1080**, 126–134.

Yip,K.S.P. *et al.* (1995) The structure of *Pyrococcus furiosus* glutamate dehydrogenase reveals a key role for ion-pair networks in maintaining enzyme stability at extreme temperatures. *Structure*, **3**, 1147–1158.

*Received February 19, 1998; revised March 20, 1998; accepted March 24, 1998*